

Ultrasensitive force detection with a nanotube mechanical resonator

J. Moser, J. Güttinger, A. Eichler, M. J. Esplandiu, D. E. Liu, M. I. Dykman, and A. Bachtold

1 Power spectrum of the current through a vibrating nanotube

We consider the power spectrum of a suspended nanotube in the presence of gate voltage that has a large DC component and a small AC component at a frequency close to the frequency of the eigenvibrations of the nanotube.

1.1 AC conductance of the vibrating nanotube

We assume that (i) the nanotube conductance is a function only of the total charge q of the nanotube, (ii) the charge distribution along the nanotube is independent of the gate voltage V_g , and (iii) the system is in the adiabatic limit, i.e. the vibration dynamics is much slower than the electron dynamics. Then q is related to the static gate voltage V_g by the capacitance C_g . We consider the effect on conductance of the bending mode of the nanotube which is polarized in the direction z perpendicular to the gate.

Based on the above assumptions we write the conductance as

$$G(q(t)) \simeq G(q_0) + \frac{\partial G}{\partial q} \delta q(t). \quad (1)$$

Quite generally, in the adiabatic limit the charge increment $\delta q(t)$ is a function of the time-dependent (AC) increment of the gate voltage $\delta V_g(t)$ and the (AC) vibrational displacement $\delta z(t)$, which is the displacement of the nanotube at the antinode of the vibrational mode. For small $|\delta V_g|$ and $|\delta z|$

$$\delta q(t) \simeq \left(\frac{\partial q}{\partial V_g} \right)_z \delta V_g(t) + \left(\frac{\partial q}{\partial z} \right)_{V_g} \delta z(t). \quad (2)$$

The AC displacement δz can be separated into the fluctuating part for constant V_g and the δV_g -induced part

$$\begin{aligned}\delta z(t) &= \delta z^{fl}(t) + \delta z^{ind}(t) & \delta z^{fl}(t) &= [\delta z(t)]_{V_g}, \\ \delta z^{ind}(t) &= \int_{-\infty}^t \frac{\delta z(t')}{\delta V_g(t')} \delta V_g(t') dt'.\end{aligned}\quad (3)$$

Since the charge and the gate potential are related by the capacitance C_g , which depends on the position of the nanotube and thus on the vibrational displacement, $C_g \equiv C_g(z)$, from Eqs. (2) and (3)

$$\delta q(t) = C_g \delta V_g(t) + (\partial_z C_g)_{V_g} V_g^{DC} \delta z^{fl}(t) + (\partial_z C_g)_{V_g} V_g^{DC} \delta z^{ind}(t), \quad (4)$$

where $\partial_z C_g$ is the derivative of the capacitance with respect to the vibration displacement calculated for zero displacement and V_g^{DC} is the DC part of the gate voltage. From Eqs. (1) and (4), the AC component of the conductance $\delta G(t) = \partial_q G \delta q(t)$ is directly related to the vibration displacement.

One can estimate the AC-gate voltage induced displacement $\delta z^{ind}(t)$ by modeling the nanotube vibrational mode by a harmonic oscillator with equation of motion

$$\delta \ddot{z}^{ind} + 2\Gamma \delta \dot{z}^{ind} + \omega_0^2 \delta z^{ind} = \frac{F \cos(\omega_G t)}{M}, \quad F = \partial_z C_g V_g^{DC} V_g^{AC}, \quad (5)$$

where M is the mass of the nanotube, $2\Gamma = \omega_0/Q$ is the decay rate of the oscillator with quality factor Q , and F is the AC force amplitude. The stationary solution of this equation is

$$\delta z^{ind}(t) = A^{ind}(\omega_G) \cos(\omega_G t - \phi), \quad A^{ind}(\omega_G) = \frac{F/M}{\sqrt{(\omega_0^2 - \omega_G^2)^2 + 4\Gamma^2 \omega_G^2}}, \quad \phi = \arctan\left(\frac{2\Gamma \omega_G}{\omega_0^2 - \omega_G^2}\right). \quad (6)$$

On resonance $\omega_G = \omega_0$, and therefore the maximal amplitude is $A_m^{ind} = F/(2M\Gamma\omega_0)$, i.e.,

$$A_m^{ind} = \partial_z C_g V_g^{DC} V_g^{AC} / 2M\Gamma\omega_0. \quad (7)$$

For classical vibrations, where $k_B T \gg \hbar\omega_0$ (in the experiment $\hbar\omega_0/k_B \sim 3 \times 10^{-4}$ K was much less than the temperature), one can estimate the root mean square amplitude A^{fl} of the fluctuating part of the displacement δz^{fl} from the expression $M\omega_0^2(A^{fl})^2/2 \sim k_B T$,

$$A^{fl} \simeq \sqrt{2k_B T / M\omega_0^2}. \quad (8)$$

We now compare the three terms in Eq. (4) for the AC charge on the resonator. We use for the estimate the typical experimental parameters $T = 1.2$ K, $V_g^{DC} = 1.45$ V, $V_g^{AC} = 200$ nV, $M = 1 \times 10^{-20}$ kg, $\omega_0 = \omega_G = 2\pi \times 5.5$ MHz, $Q = 48,000$, $C_g = 1.8 \times 10^{-17}$ F, and $\partial_z C_g = 1.2 \times 10^{-12}$ F/m. We start with the ratio of the third term and the first term,

$$\frac{(\partial_z C_g) V_g^{DC} \delta z^{ind}}{C_g V_g^{AC}} \sim \frac{(\partial_z C_g)^2 (V_g^{DC})^2}{C_g M \omega^2} \times Q \simeq 700 \gg 1. \quad (9)$$

Therefore, when an AC gate voltage resonates with vibrations of the nanotube, its effect on the AC conductivity comes primarily through the excitation of the vibrations rather than through direct modulation. Respectively, we will disregard the first term in Eq. (4).

We now compare the third and the second terms in Eq. (4). On exact resonance

$$\frac{(\partial_z C_g) V_g^{DC} \delta z^{ind}}{(\partial_z C_g) V_g^{DC} \delta z^{fl}} = \frac{A_m^{ind}}{A^{fl}} \sim 1. \quad (10)$$

Therefore in the conditions of the experiment the AC conductance is

$$\delta G(t) = \partial_q G \delta q(t) \simeq \partial_q G (\partial_z C_g)_{V_g} V_g^{DC} (\delta z^{fl}(t) + \delta z^{ind}(t)). \quad (11)$$

The experimentally observable characteristic is the transconductance, dG/dV_g . It is usually defined with respect to slowly varying V_g . In the case of vibrations with a large quality factor a slow variation of V_g does not lead to excitation of the vibrations. Then one has

$$\partial_q G \approx C_g^{-1} dG/dV_g. \quad (12)$$

This expression is used in the main text.

1.2 Current power spectrum

If we neglect the effect of delay, i.e. if the current depends only on the instantaneous conductance, the current change due to the AC gate modulation is

$$\delta I(t) = \delta G(t) V_{sd}(t), \quad (13)$$

where V_{sd} is the source-drain voltage. If $V_{sd}(t) = V_{sd}^{DC} = \text{const}$,

$$\delta I(t) \simeq \partial_q G (\partial_z C_g)_{V_g} V_g^{DC} V_{sd}^{DC} (\delta z^{fl}(t) + A^{ind}(\omega_G) \cos(\omega_G t - \phi)). \quad (14)$$

The autocorrelation function of the current is defined as

$$\begin{aligned}\bar{P}_I(\tau) &= \langle \delta I(t+\tau)\delta I(t) \rangle = \lim_{T \rightarrow \infty} \frac{1}{2T} \int_{-T}^T \delta I(t+\tau)\delta I(t) dt \\ &= \left(\partial_q G (\partial_z C_g)_{V_g} V_g^{DC} V_{sd}^{DC} \right)^2 \left(\langle \delta z^{fl}(\tau)\delta z^{fl}(0) \rangle + \frac{1}{2} (A^{ind}(\omega_G))^2 \cos(\omega_G \tau) \right).\end{aligned}\quad (15)$$

Then the power spectrum of the current for $\omega \geq 0$ can be written as

$$\begin{aligned}P_I(\omega) &= \left(\partial_q G (\partial_z C_g)_{V_g} V_g^{DC} V_{sd}^{DC} \right)^2 (P^{fl}(\omega) + P^{ind}(\omega)), \\ P^{fl}(\omega) &= \frac{1}{2\pi} \int_{-\infty}^{\infty} d\tau e^{i\omega\tau} \langle \delta z^{fl}(\tau)\delta z^{fl}(0) \rangle, \quad P^{ind}(\omega) = A^{ind}(\omega_G)^2 \frac{\delta(\omega - \omega_G)}{4}.\end{aligned}\quad (16)$$

Here, $P^{fl}(\omega)$ is the spectrum of the oscillator due to thermal fluctuations. It shows a peak at resonant frequency ω_0 with width ω_0/Q . In $P_I(\omega)$ there is also a delta function due to the periodic AC gate potential with area $\propto A^{ind}(\omega_G)^2$.

If the source-drain voltage is a periodic function of time, $V_{sd}(t) = V_{sd}^{AC} \cos(\omega_{sd}t)$, the current autocorrelation function becomes

$$\bar{P}_I^{AC}(\tau) = \frac{1}{2} \left(\partial_q G (\partial_z C_g)_{V_g} V_g^{DC} V_{sd}^{AC} \right)^2 \left(\langle \delta z^{fl}(\tau)\delta z^{fl}(0) \rangle \cos(\omega_{sd}\tau) + \frac{1}{2} A^{ind}(\omega_G)^2 \sum_{\alpha=\pm} \cos((\omega_G + \alpha\omega_{sd})\tau) \right).\quad (17)$$

In the frequency range of interest, $\omega_0 \gg \omega > 0$, the power spectrum can be written as

$$P_I^{AC}(\omega) = \frac{1}{4} \left(\partial_q G (\partial_z C_g)_{V_g} V_g^{DC} V_{sd}^{AC} \right)^2 \left(P^{fl}(\omega - \omega_{sd}) + \frac{1}{2} P^{ind}(\omega - |\omega_G - \omega_{sd}|) \right).\quad (18)$$

The modulating source-drain voltage shifts the peaks in the power spectrum by $\pm\omega_{sd}$. Equation (2) in the main text is obtained from Eqs. (16) and (18) using $\partial_q G = C_g^{-1} \partial_{V_g} G$ (see Eq. (12)).

1.3 Current power spectrum in the presence of frequency noise

In the presence of frequency noise, the oscillator can be described by

$$\begin{aligned}\delta \ddot{z} + 2\Gamma\delta\dot{z} + [\omega_0^2 + 2\omega_0\xi(t)]\delta z &= \frac{F \cos(\omega_G t) + f(t)}{M} \\ \langle f(t)f(t') \rangle &= 4M\Gamma k_B T \delta(t - t'),\end{aligned}\quad (19)$$

where F is given by Eq. (5) and $f(t)$ describes a white thermal Gaussian noise. The noise $\xi(t)$ is the frequency noise. The frequency noise can have various origins, such as charge fluctuations and weak nonlinear coupling to other eigenmodes; it can be of thermal or non-thermal nature. For high quality factor vibrations, it is reasonable to model it by a Gaussian noise with a bandwidth that largely exceeds the decay rate Γ , but is small compared to the vibration eigenfrequency ω_0 . Such noise is effectively white in the rotating frame.

For Γ and $|\omega_G - \omega_0|$ much smaller than ω_0 one can analyze the problem in the rotating frame using a standard transformation

$$\delta z(t) = u(t) e^{i\omega_G t} + u^*(t) e^{-i\omega_G t}, \quad \delta \dot{z}(t) = i\omega_G (u(t) e^{i\omega_G t} - u^*(t) e^{-i\omega_G t}). \quad (20)$$

The equation of motion for the complex amplitude u reads

$$\dot{u} \simeq -(\Gamma + i\delta\omega - i\xi(t)) u - \frac{iF}{4M\omega_G} + f_u(t), \quad (21)$$

where $\delta\omega = \omega_G - \omega_0$ and $f_u(t) = -(i/2M\omega_G)f(t)\exp(-i\omega_G t)$. The solution can be conveniently written in the form [2]

$$\begin{aligned} u(t) &= u^{ind}(t) + u^{fl}(t) \\ u^{ind}(t) &= \frac{F}{4M\omega_G} \int_{-\infty}^t dt_1 \chi^*(t-t_1) \exp \left[i \int_{t_1}^t dt'_1 \xi(t'_1) \right] \\ u^{fl}(t) &= i \int_{-\infty}^t dt_1 \chi^*(t-t_1) f_u(t_1) \exp \left[i \int_{t_1}^t dt'_1 \xi(t'_1) \right], \end{aligned} \quad (22)$$

where $\chi(t) = i \exp[-(\Gamma - i\delta\omega)t]$. The terms with u^{fl} and u^{ind} give, respectively, the spontaneous and induced parts of the vibrational displacement δz^{fl} and δz^{ind} . In the "slow" time compared to the reciprocal frequencies $\omega_0^{-1}, \omega_G^{-1}$ the noise $\xi(t)$ is δ -correlated, that is, in Eq. (22) one can set $\langle \xi(t)\xi(t') \rangle = 2D\delta(t-t')$.

As a result of frequency fluctuations, the expressions for the power spectra $P^{fl}(\omega)$ and $P^{ind}(\omega)$ of the spontaneous fluctuations and the V_g^{AC} -induced motion are modified. We start with the induced contribution. Taking into account that the noise $\xi(t)$ is Gaussian, we have for $\tau > 0$

$$\begin{aligned} \bar{P}^{ind}(\tau) &= \langle u^{ind}(\tau)(u^{ind}(0))^* \rangle e^{i\omega_G \tau} + \langle (u^{ind}(\tau))^* u^{ind}(0) \rangle e^{-i\omega_G \tau} \\ &= \left(\frac{F}{4M\omega_G} \right)^2 \int_{-\infty}^{\tau} dt_1 \chi^*(\tau-t_1) \int_{-\infty}^0 dt_2 \chi(-t_2) e^{-\Xi(t_1, t_2; \tau)} e^{i\omega_G \tau} + c.c. \\ &= \left(\frac{F}{4M\omega_G} \right)^2 \frac{1 + (D/\Gamma) \exp[-(\Gamma + D + i\delta\omega)\tau]}{(\omega_G - \omega_0)^2 + (\Gamma + D)^2} e^{i\omega_G \tau} + c.c. \end{aligned} \quad (23)$$

Here, $\Xi(t_1, t_2; \tau) = D(\tau - t_1 - t_2)\Theta(t_1) + D(\tau + |t_1 - t_2|)\Theta(-t_1)$, where $\Theta(x)$ is the step function. We note that, unexpectedly, phase noise imposes correlations of the response, so that $\langle u^{ind}(\tau)(u^{ind}(0))^* \rangle$ along with the term $|\langle u^{ind}(\tau) \rangle|^2$ has a term that exponentially decays in time.

As seen from Eq. (23), the pronounced feature in the power spectrum of modulated vibrations is the δ -shape peak. On exact resonance, $\omega_G = \omega_0$, for $\omega > 0$

$$P^{ind}(\omega) = \frac{F^2}{16M^2\omega_G^2(\Gamma + D)^2} \left[\delta(\omega - \omega_G) + \frac{D}{\pi\Gamma} \frac{\Gamma + D}{(\Gamma + D)^2 + (\omega - \omega_G)^2} \right]. \quad (24)$$

A well-known result for the correlation function of thermally induced fluctuations is

$$P^{fl}(\tau) = \langle u^{fl}(\tau)(u^{fl}(0))^* \rangle e^{i\omega_G\tau} + c.c. = \frac{k_B T}{2M\omega_G^2} e^{i\omega_0\tau - (\Gamma + D)|\tau|} + c.c., \quad (25)$$

and the power spectrum is, respectively,

$$P^{fl}(\omega) = \frac{k_B T}{2\pi M\omega_G^2} \frac{\Gamma + D}{(\omega - \omega_0)^2 + (\Gamma + D)^2}. \quad (26)$$

The spectral peak (26) is Lorentzian with full width at half-maximum (in Hz)

$$\Gamma_{\text{meas}} = (\Gamma + D)/\pi, \quad (27)$$

and is associated to the force sensitivity

$$S_F = 8\pi M k_B T \Gamma_{\text{meas}}. \quad (28)$$

We emphasize that the fluctuation-dissipation theorem applies in the presence of frequency noise. Indeed if, using Eq. (19), one introduces the susceptibility $\alpha(\omega_G)$ by the relation $\langle \delta z \rangle = (1/2)\alpha(\omega_G)F \exp(-i\omega_G t) + c.c.$ and derives $\alpha(\omega_G)$ directly from Eq. (22), one finds that

$$\text{Im } \alpha(\omega_G) = (\pi\omega_G/k_B T)P^{fl}(\omega_G).$$

We compare the area (integral over the frequency $\omega > 0$) s^{ind} of the δ -peak of $P^{ind}(\omega)$ to the measured area s^{fl} of the spectral peak in the absence of modulation. We note that the area of the peak in P^{ind} is given by $|\alpha(\omega_G)|^2 F^2/4$,

in agreement with Eq. (24). From Eqs. (24) and (26) we see that

$$\frac{s^{fl}}{s^{ind}} = \frac{\pi\Gamma_{\text{meas}}S_F}{F^2}. \quad (29)$$

1.4 Measuring S_F

Making contact with the experiment illustrated in Fig. 4 of the main text goes as follows:

- We express F and V_g^{AC} in terms of their rms values: $F = \sqrt{2}F_{\text{rms}}$, $V_g^{AC} = \sqrt{2}V_{g,\text{rms}}^{AC}$.
- s^{fl} is the area of the thermal resonance in the Fourier spectrum of the current cross-correlation $\langle \delta I^2 \rangle^{fl}(f)$ divided by the measurement resolution bandwidth rbw: $s^{fl} = \frac{1}{\text{rbw}} \int_0^\infty \langle \delta I^2 \rangle^{fl}(f) df$.
- The driven signal is a sharp peak superimposed on the thermal resonance. The area of the driven signal associated to the sharp peak is $s^{ind} = \frac{1}{\text{rbw}} \int_0^\infty \langle \delta I^2 \rangle^{ind}(f) df$. Because the driving force is modulated at a frequency that is defined within the resolution bandwidth of our vector signal analyzer, all the power of this force is contained within rbw. Defining $(I_{\text{peak}})^2$ as the height of the driven signal in the Fourier spectrum of the current cross-correlation, we obtain $s^{ind} = (I_{\text{peak}})^2$.

Hence, Eq. (29) becomes:

$$S_F = \frac{2F_{\text{rms}}^2}{\pi\Gamma_{\text{meas}}} \times \frac{s^{fl}}{s^{ind}} \quad (30)$$

$$= \frac{2F_{\text{rms}}^2}{\pi\Gamma_{\text{meas}}} \times \frac{1}{\text{rbw}} \frac{\int_0^\infty \langle \delta I^2 \rangle^{fl}(f) df}{(I_{\text{peak}})^2}, \quad (31)$$

where $F_{\text{rms}} = C'_g V_g^{DC} V_{g,\text{rms}}^{AC} \sin \theta$. Now, assuming that the thermal resonance has a Lorentzian lineshape, we can also express Eq. (31) in a form that is directly applicable to the experiment shown in Fig. 4 of the main text:

$$S_F = \frac{\text{thermal resonance height}}{\text{driven peak height}} \times (C'_g V_g^{DC} V_{g,\text{rms}}^{AC} \sin \theta)^2 \times \frac{1}{\text{rbw}}, \quad (32)$$

where the heights refer to $\langle \delta I^2 \rangle(f)$ spectra (not to $S_I(f)$ spectra). Equation (32) is valid whether fluctuations in frequency are present or not.

- Equation (32) can be understood as follows. The force sensitivity can be simply determined from the applied

force when the signal-to-noise ratio is one (SNR = 1). That is,

$$S_F \times \text{rbw} = F_{\text{rms}}^2 \text{ when } \frac{\text{thermal resonance height}}{\text{driven peak height}} = 1.$$

- We verified that the output of the Fourier transform of the cross-correlation of our vector signal analyzer is well calibrated both for an input signal with large bandwidth and for a delta peak. The former is necessary to properly quantify the term "(thermal resonance height)/rbw" in Eq. (32) and the latter to quantify the term "driven peak height". For this, we measured (i) the Johnson-Nyquist noise of the 2 kOhm resistor away from any mechanical resonances, and (ii) the cross-correlation of a known signal $V^{AC} \cos(2\pi f_0 t)$.

2 Device characteristics

2.1 Estimating the effective mass of mode 1 and mode 2

Because mode 1 and mode 2 are degenerate at low gate voltage (see Fig. 1c of the main text), we consider that both modes have the same effective mass M . The effective mass of these modes is related to the mass of the nanotube M_{NT} as

$$M = M_{NT} \frac{1}{L} \int_0^L [\phi(x)]^2 dx, \quad (33)$$

where L is the length of the nanotube and $\phi(x)$ is the shape of the mode, which is normalized so that $\max[\phi(x)] = 1$. Applying a voltage to the gate bends the nanotube towards the gate, and thus induces mechanical tension in it. As a result, the shape of the fundamental mode can be approximated as $\phi(x) = \sin(\pi x/L)$, hence $M = M_{NT}/2$. We estimate M_{NT} from the size of the nanotube measured by atomic force microscopy. The distance between source and drain electrodes is $L = 4 \pm 0.1 \mu\text{m}$. The diameter of the nanotube is $d = 2.1 \pm 0.5 \text{ nm}$. From these values, we estimate the effective mass of the two fundamental eigenmodes mode 1 and mode 2 to be

$$M = \frac{1}{2} \left(2M_C \times \frac{\pi d \times L}{A} \right) = 9.8 \times 10^{-21} \pm 2.4 \times 10^{-21} \text{ kg}, \quad (34)$$

where M_C is the mass of a carbon atom and $A = 5.2 \times 10^{-20} \text{ m}^2$ is the surface area of a hexagon in the honeycomb lattice of graphene.

2.2 Calculating C'_g

We assume that the capacitance C_g between the nanotube and the gate is described by

$$C_g = \frac{2\pi\epsilon_0 L}{\ln\left(\frac{4(h-z)}{d}\right)}, \quad (35)$$

where ϵ_0 is the vacuum permittivity, $h = 2 \pm 0.4 \mu\text{m}$ is the effective separation between the nanotube and the gate, and d is the diameter of the nanotube. The derivative of C_g with respect to a displacement normal to the gate (z direction) reads

$$C'_g = \left(\frac{dC_g}{dz}\right)_{z=0} = \frac{C_g}{h \ln(4h/d)}. \quad (36)$$

The capacitance C_g is estimated from the average gate bias spacing between two subsequent Coulomb blockade peaks. As a result, we obtain

$$C'_g = 1.2 \times 10^{-12} \pm 0.4 \times 10^{-12} \text{ F/m}. \quad (37)$$

2.3 Detecting the thermal motion

Figure S1 displays a schematic of our measurement setup. Current fluctuations δI are converted into voltage fluctuations across a resistor $R = 2 \text{ k}\Omega$. These voltage fluctuations are amplified by a two-stage amplification scheme along two parallel lines. Each two-stage amplification scheme consists of a low-noise, high-impedance voltage amplifier (LI-75A, NF Corporation) of gain 100 at the first stage, and a Stanford Research amplifier SR560 set to a gain of 50 at the second stage. We send the output of the SR560 amplifiers to a fast Fourier transform signal analyzer (HP 89410A). The signal analyzer acquires data in time domain, and calculates the cross-correlation; its output is the Fourier transform $\langle V_A V_B \rangle$ of this cross-correlation. The voltage noise V_{NA} and V_{NB} of the two

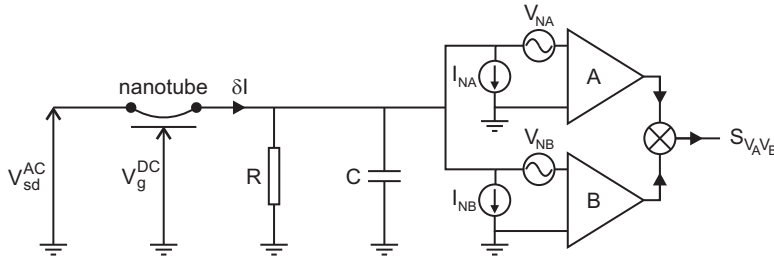


Figure S1: Detailed schematic of the experimental setup. Elements added to Fig 2a of the main text: capacitance C of the measuring lines, amplifier's current noise $I_{NA,NB}$, amplifier's voltage noise $V_{NA,NB}$. The output signal of the vector signal analyzer is $S_{V_A V_B}$, the power spectral density of the cross-correlation of the output voltages of amplifiers A and B. We convert $S_{V_A V_B}$ into S_I using Eq. (38).

amplifiers cancel out in the cross-correlation. The power spectral density of voltage fluctuations at the output of the amplifiers is $S_{V_A V_B} = \langle V_A V_B \rangle / \text{rbw}$, where rbw is the resolution bandwidth of the measurement. It can be expressed as [1]

$$S_{V_A V_B} = [\Lambda(f) \times (S_I + S_{I_R} + 2S_{I_{NA, NB}})R^2 + S_{\text{offset}}] \times \text{gain}. \quad (38)$$

Note that in the above expression, we define $S_I(f) = \int_{-\infty}^{+\infty} d\tau e^{i2\pi f\tau} \langle I(\tau)I(0) \rangle$, so that $S_I(f) \equiv 2\pi P_I^{AC}(2\pi f)$ in the notations of Eq. (18). Here, S_I is the power spectral density of the current fluctuations at the drain, $S_{I_R} = 4k_B T/R$ is the Johnson-Nyquist noise of the resistor, $S_{I_{NA, NB}}$ is the amplifier current noise and S_{offset} is a voltage noise offset. $\Lambda(f) = \frac{1}{1+(2\pi fRC)^2}$ is a frequency dependent attenuation factor, which accounts for the RC filtering of the lines inside the cryostat. Fitting the background of $S_{V_A V_B}(f)$ to Eq. (38), we extract $C = 1.6$ nF and $S_{\text{offset}} = 9 \times 10^{-20}$ V²/Hz. The voltage noise offset is comparable to $S_{\text{offset}} = 10.8 \times 10^{-20}$ V²/Hz measured by Choi et al. [1] and is attributed to residual crosstalk between the amplifiers. We use a total gain of 2.5×10^7 , which accounts for an amplification of $100\times$ for each LI-75A and of $50\times$ for each Stanford Research 560. The current noise of the LI-75A amplifier is specified to be $S_{I_{NA, NB}} < 2 \times 10^{-28}$ A²/Hz. Hence the current noise of the amplifier does not significantly contribute to our output signal, as it corresponds to a voltage noise of $2S_{I_{NA, NB}}R^2 = 1.6 \times 10^{-21}$ V²/Hz (or a noise temperature of 0.1 mK in combination with our 2k Ω resistor).

The power spectral density of electro-mechanical current fluctuations is given by

$$S_I(f) = \frac{\langle \delta I^2 \rangle(f)}{\text{rbw}}, \quad (39)$$

where $\langle \delta I^2 \rangle(f)$ is the Fourier transform of the cross-correlation of current fluctuations. We obtain

$$S_I(f) = \beta^2 S_z(f), \quad (40)$$

where $S_z(f)$ is the power spectral density of the projection along z of displacement fluctuations and β is defined as

$$\beta = \frac{1}{2} \frac{dG}{dV_g} V_g^{DC} V_{sd}^{AC} \frac{C'_g}{C_g}. \quad (41)$$

2.4 Estimating the angle θ

We can estimate the angle θ by assuming that modes 1 and 2 have the same thermal energy. According to the equipartition theorem,

$$k_B T = 4\pi^2 f_1^2 M \langle \delta r_1^2 \rangle = 4\pi^2 f_2^2 M \langle \delta r_2^2 \rangle, \quad (42)$$

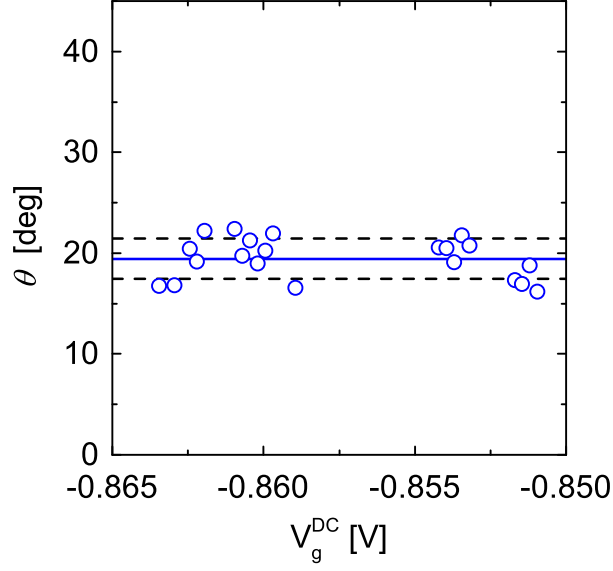


Figure S2: Angle θ as a function of voltage applied to the gate V_g^{DC} . The blue line shows the mean value of 19.5° . The dashed lines indicate the standard deviation of 2° .

where $f_{1,2}$ and $\langle \delta r_{1,2}^2 \rangle$ are the resonant frequencies and the variances of the displacement for the two modes. Since our detection technique is only sensitive to the motional component along the z direction, we express $\langle \delta r_1^2 \rangle$ and $\langle \delta r_2^2 \rangle$ in terms of the variances of the projections of the displacements along z (see inset to Fig. 1c of the main text):

$$\begin{aligned} \langle \delta z_1^2 \rangle &= \langle \delta r_1^2 \rangle \sin^2 \theta, \\ \langle \delta z_2^2 \rangle &= \langle \delta r_2^2 \rangle \cos^2 \theta. \end{aligned} \quad (43)$$

In addition, $\langle \delta z_{1,2}^2 \rangle$ are proportional to the variance of electro-mechanical current fluctuations at the drain (see Eqs. (40) and (41)):

$$\langle \delta z_{1,2}^2 \rangle = \left(\frac{1}{\beta} \right)^2 \langle \delta I_{1,2}^2 \rangle. \quad (44)$$

Provided that mode 1 and mode 2 are measured with the same values of V_{sd}^{AC} and V_g^{DC} , we can use Eqs. (43) and (44) to express Eq. (42) as

$$\frac{f_{01}^2}{\sin^2 \theta} \langle \delta I_1^2 \rangle = \frac{f_{02}^2}{\cos^2 \theta} \langle \delta I_2^2 \rangle, \quad (45)$$

where $\langle \delta I_1^2 \rangle$ and $\langle \delta I_2^2 \rangle$ are the variances of electro-mechanical current fluctuations measured for mode 1 and mode 2, respectively. These variances can also be expressed in terms of the areas under the S_{I_1} and S_{I_2} spectra, where $S_{I_{1,2}}$

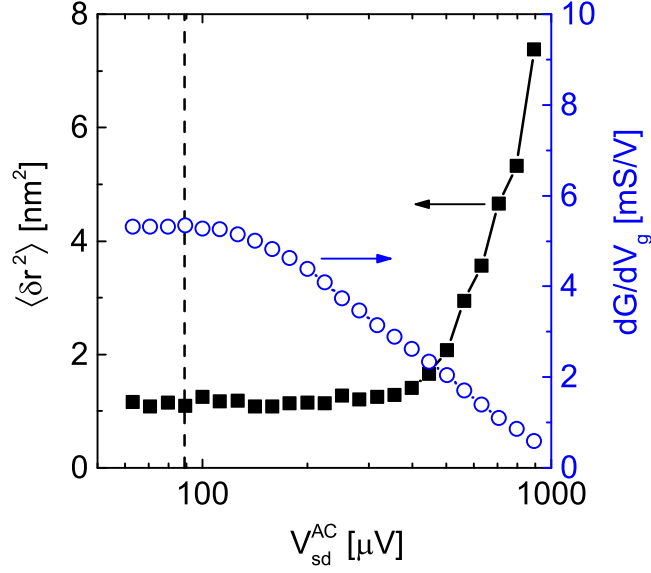


Figure S3: Variance $\langle \delta r^2 \rangle$ (black squares) and transconductance dG/dV_g (blue circles) as a function of V_{sd}^{AC} for mode 1 at 1.2 K. As explained in section 3, the variance reads $\langle \delta r^2 \rangle = \frac{1}{\beta^2 \cos^2 \theta} \int_0^\infty S_I(f) df$. We measured S_I using the following parameters: $f_{sd} = 5.61$ MHz (frequency of $V_{sd}(t)$), $rbw = 9.375$ Hz, $V_g^{DC} = -0.854$ V, and 56 dB attenuation. To calculate $\langle \delta r^2 \rangle$, we used $\theta = 19.5^\circ$, nanotube-gate capacitance $C_g = 1.8 \times 10^{-17}$ F, $C'_g = 1.2 \times 10^{-12}$ F/m, cable capacitance $C = 1.6$ nF (see section 2.3), and $dG/dV_g = 1.2$ mS/V.

are the power spectral densities of current fluctuations for the two modes:

$$\langle \delta I_{1,2}^2 \rangle = \int_0^\infty S_{I_{1,2}}(f) df.$$

Hence Eq. (45) can be expressed as

$$\tan \theta = \frac{f_{01}}{f_{02}} \sqrt{\frac{\int_0^\infty S_{I_1}(f) df}{\int_0^\infty S_{I_2}(f) df}}. \quad (46)$$

The S_I spectra for mode 1 and mode 2, measured at 1.2 K and at various V_g^{DC} values, allow us to extract θ using Eq. (46). As shown in Fig. S2, $\theta = 19.5^\circ \pm 2^\circ$ in the range of V_g^{DC} values we used in the measurements.

2.5 Dependence of thermal resonances on V_{sd}^{AC}

In this section, we demonstrate that the AC voltage we apply between source and drain to read out the electro-mechanical current does not increase the temperature of the modes under study. In other words, we show that the values of V_{sd}^{AC} we use throughout our work does not affect the outcome of our experiment. Figure S3 shows the displacement variance $\langle \delta r^2 \rangle$ for mode 1 along with the transconductance dG/dV_g as a function of V_{sd}^{AC} . The transconductance is extracted from measurements of the DC source-drain current as a function of V_{sd}^{AC} ; it is

smoothed to ease readability. The dashed line corresponds to $V_{sd}^{AC} = 89 \mu\text{V}$ used in Fig. 2 of the main text. Using a range of V_{sd}^{AC} over which (1) the variance and (2) the transconductance are constant ensures that (1) the temperature of the mode and (2) the electron temperature are unaffected by the measurement.

3 Variance of displacement as a function of temperature

To measure the variance of displacement as a function of temperature, we consider mode 2, whose thermal resonance can be resolved up to at least 6 K. Using Eqs. (40) and (41), we derive the power spectral density S_r of the displacement fluctuations δr :

$$S_r = \frac{1}{\beta^2 \cos^2 \theta} S_I. \quad (47)$$

The variance of δr reads

$$\langle \delta r^2 \rangle = \int_0^\infty S_r(f) df = \frac{1}{\beta^2 \cos^2 \theta} \int_0^\infty S_I(f) df. \quad (48)$$

Figure S4 shows the standard deviation of the displacement $\delta r = \sqrt{\langle \delta r^2 \rangle}$, the quality factor Q , and the conductance G as a function of gate bias V_g^{DC} at 1.2, 3 and 6 K. We measure S_I using expression (38). The transconductance $\frac{dG}{dV_g}$ as a function of V_g^{DC} is determined in a separate measurement. We found that $\frac{dG}{dV_g}(V_g^{DC})$ traces shift in V_g^{DC} by a fraction of mV from one measurement to the next. Even though these shifts are later corrected by comparing $\frac{dG}{dV_g}(V_g^{DC})$ and $S_I(V_g^{DC})$ traces, the calculation of δr from Eq. (48) may still contain a spurious V_g^{DC} dependence, especially at 1.2 K where the transconductance strongly depends on V_g^{DC} . Since δr should not depend on V_g^{DC} according to the equipartition theorem, we calculate the average of δr over the range of V_g^{DC} shown in Fig. S4. The result of this average, plotted as a function of temperature, is shown in Fig. S5. The temperature dependence of the variance is consistent with the equipartition theorem $4\pi^2 f_0^2 M \langle \delta r^2 \rangle = k_B T$.

4 Non-thermal force noise

Improving the force sensitivity of carbon nanotube resonators towards the $1 \text{ zN}/\sqrt{\text{Hz}}$ scale will require minimizing non-thermal force noises which might become non-negligible. Non-thermal forces are different from the fluctuating Langevin forces in that they are not related to the dissipation of the resonator (via the fluctuation-dissipation theorem). Due to the strong electrostatic coupling of the nanotube to the gate, we consider two noise processes of electrostatic origin.

One source of non-thermal force noise could be related to the Johnson-Nyquist noise of the electrical circuit. The latter translates into an electrostatic force noise $S_{JN} = 4k_B T R (C'_g V_g^{DC} \sin \theta)^2 = 0.2 \text{ zN}/\sqrt{\text{Hz}}$ at 1.2 K where

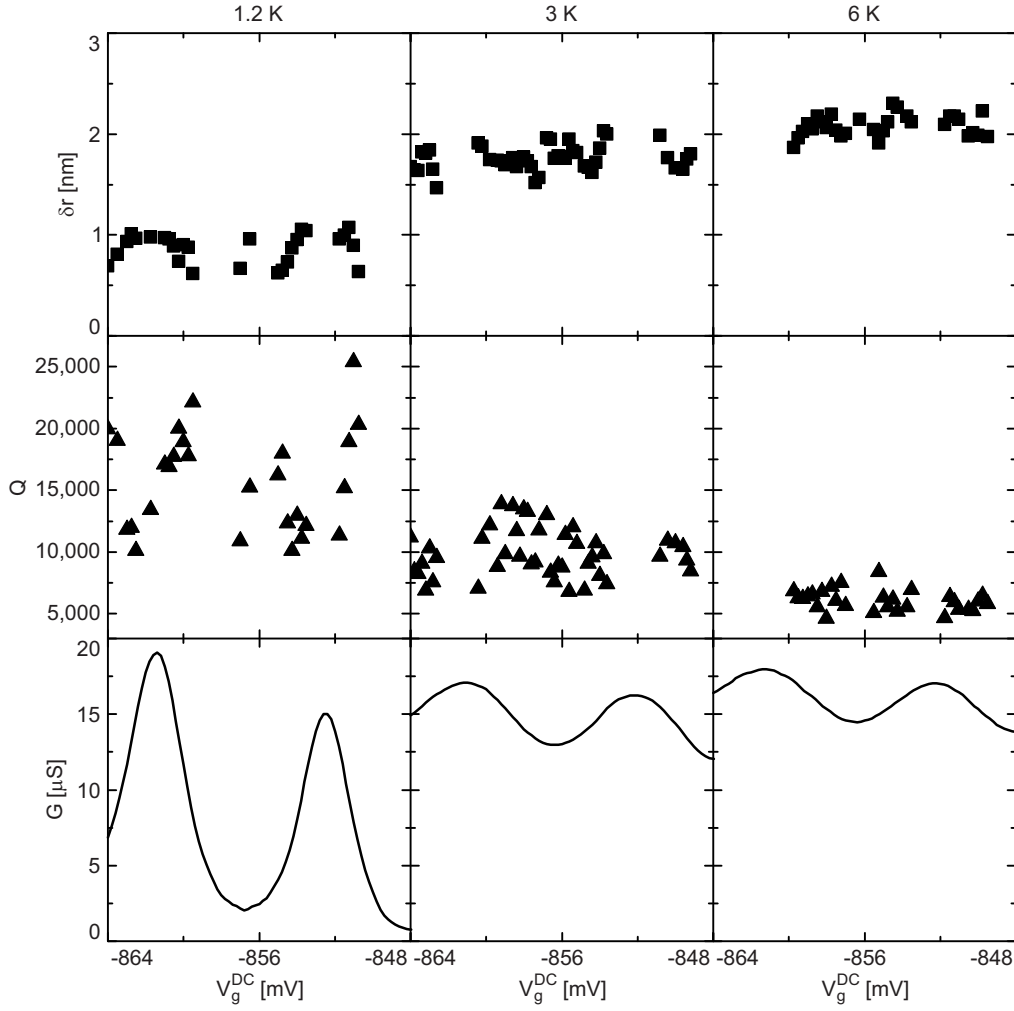


Figure S4: Standard deviation of the displacement $\delta r = \sqrt{\langle \delta r^2 \rangle}$, quality factor Q , and conductance G as a function of V_g^{DC} . Each data point corresponds to a well-defined $S_I(f)$ spectrum, which could be properly fitted to a Lorentzian function.

R is the 2 k Ω resistor. This force noise can be further reduced by lowering the temperature.

A second source of non-thermal force noise could be related to the single-electron charging-discharging process in the Coulomb blockade regime. In this regime, electrons are strongly coupled to the motion of the nanotube [3, 4]. At a fixed V_g^{DC} value, the nanotube experiences single-electron charging and discharging events whose statistic is that of telegraph noise. Because the rates at which these events occur are much higher than the mechanical frequency of the nanotube (see below), the resulting electrostatic force noise can be considered to be white, and its power spectral density reads [5]

$$S_{F_e} = F_e^2 \times 4 \frac{W_{in} W_{out}}{(W_{in} + W_{out})^3}, \quad (49)$$

where the telegraph force takes the values $\pm F_e = \pm(e/2)V_g^{DC} \sin \theta(C'_g/C_{tube})$, and $W_{in,out}$ are the rates for the

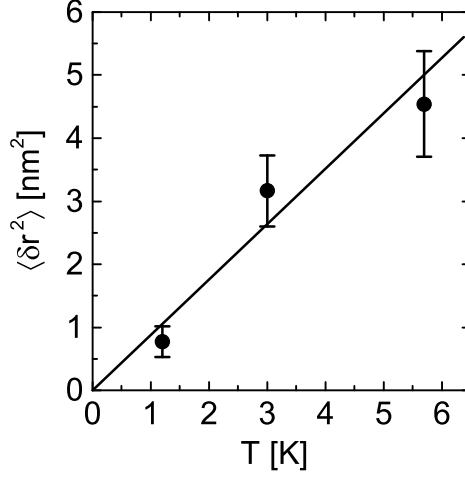


Figure S5: Variance of the displacement of mode 2 as a function of temperature. The straight line is a fit to $k_B T / (4\pi^2 f_0^2 M)$ using $f_0 = 6.3$ MHz and $M = 9.8 \times 10^{-21}$ kg.

electron to jump on and off the nanotube, respectively. Here, C_{tube} is the capacitance of the nanotube dot; it is related to the nanotube-gate capacitance as $C_{tube} = C_g / \alpha_g$, where $\alpha_g = 0.2$ is the lever arm between the nanotube and the gate electrode.

S_{F_e} depends on the tunnel rate across the two barriers that define the nanotube quantum dot. We assume that the left and right barriers have the same tunnel rate W_b . Since an electron can tunnel into or out of the nanotube from both leads, we have

$$W_{in} = 2W_b \times f, \quad W_{out} = 2W_b \times (1 - f). \quad (50)$$

Here f is the Fermi-Dirac distribution:

$$f(V_g^{DC}) = \left(1 + \exp \left(\frac{\alpha_g |e| (V_g^{DC} - V_{g,peak}^{DC})}{k_B T} \right) \right)^{-1}, \quad (51)$$

with $V_{g,peak}^{DC}$ the gate bias value corresponding to the Coulomb blockade peak in conductance. The maximum value for S_{F_e} is obtained for $V_g^{DC} = V_{g,peak}^{DC}$, and reads:

$$\max(S_{F_e}) = F_e^2 \frac{1}{2W_b}. \quad (52)$$

We estimate W_b from the peak value G_{peak} of the conductance oscillations. According to Ref. [6], $W_b = 2\Delta E \times G_{peak} / e^2$ in the limit $k_B T \gg \Delta E$, where ΔE is the level spacing; while in the opposite limit ($k_B T \ll \Delta E$), $W_b = 8k_B T \times G_{peak} / e^2$. The level spacing of the nanotube is $\Delta E = \hbar v_F / 8L = 1.6$ K with v_F the Fermi velocity

and L the dot length. Both this estimate and the temperature dependence of G_{peak} (Fig. S4) indicate that the level spacing ΔE of the nanotube is somewhat larger than $k_B T$ at 1.2 K, so that none of the above limits are reached. We therefore make the rough approximation of averaging the two limits, leading to $W_b \simeq 5k_B T \times G_{peak}/e^2 \simeq 7 \times 10^{10}$ Hz. As a result, we estimate that S_{F_e} does not exceed $\sim 1 \text{ zN}/\sqrt{\text{Hz}}$.

This non-thermal force noise can be reduced by working in the Fabry-Perot regime.

5 Detecting nuclear spins with a nanotube resonator

The force sensitivity demonstrated with our nanotube resonator might enable the detection of single nuclear spins. These spins would originate from atomic species attached to the nanotube. The coupling between the spins and the motion of the nanotube would be provided by a strong magnetic field gradient Υ . In a Magnetic Resonance Force Microscopy (MRFM) experiment, the signal-to-noise ratio (SNR) for magnetic moment detection reads

$$\text{SNR} = \frac{\sqrt{N}\mu\Upsilon}{\sqrt{S_F}}(\tau \times t_m)^{1/4}, \quad (53)$$

where N is the number of atoms with magnetic moment μ , τ is the spin correlation time, and t_m is the measurement time. If our nanotube resonator can be integrated into the experimental setups described in Ref. [7, 8] without degrading the force sensitivity achieved in the present work, it should be feasible to detect a single nuclear spin. Indeed, using parameters obtained in Ref. [8] ($\Upsilon = 4.2 \times 10^6$ T/m, $\tau = 20$ ms), we anticipate a SNR of 2 for the spin of one hydrogen atom with a measurement time of 1 s.

In the experimental setups employed in Ref. [7, 8], the strong magnetic field gradient is produced by a micromachined permanent magnet. An experimental setup that should be compatible in a straightforward manner with the fabrication process of our nanotube resonators was recently demonstrated by Nichol et al. [9, 10]. The core element of this setup is a current-carrying wire microfabricated near the nanotube [11]. This wire serves several purposes:

- it produces a radio frequency magnetic field for spin manipulation;
- it also produces a strong, oscillating magnetic field gradient $\Upsilon(t)$: this renders the use of a micromachined permanent magnet unnecessary, and enhances the spin signal by increasing the number of resonant spins.

Integrating our nanotube resonator into this setup may allow to detect the nuclear spins of ^{13}C naturally present in the nanotube. Detecting ^{13}C nuclear spins would require fabricating the nanotube resonator within close proximity to the current-carrying wire. To estimate the expected SNR, we proceed as follows. We consider the 4 μm long nanotube used in this Letter, made of $\sim 1.2 \times 10^6$ carbon atoms. We also consider a layout where the current-

carrying wire is parallel to the nanotube over a distance of $1\ \mu\text{m}$. Statistically, 1% of the carbon atoms in this $1\ \mu\text{m}$ long segment are ^{13}C , yielding $N \sim 3 \times 10^3$ ^{13}C atoms whose nuclear spins can be manipulated. Considering a nanotube-wire distance of 80 nm and a magnetic field gradient of $\Upsilon = 1.2 \times 10^5$ T/m as in Ref. [9], we estimate a force per ^{13}C atom $F_\mu = \mu_C \Upsilon = 4.2 \times 10^{-22}$ N, where $\mu_C = 3.5 \times 10^{-27}$ J/T is the magnetic moment of ^{13}C . Using $\tau = 1$ s as in Ref. [9] and $t_m = 1$ s, we obtain $\text{SNR} = 2.3$. Such a SNR should enable the detection of the spin of the ^{13}C atoms of the nanotube.

To further optimize the SNR, it may be possible to reduce the distance between the nanotube and the current-carrying wire using a DC voltage between the two. It may also be possible to apply a larger current across the wire, provided that this does not result in heating. Eventually, a clear strategy to maximize the spin signal is to fabricate resonators for which the nanotube was grown with ^{13}C -enriched methane gas.

To minimize the electrostatic drive of the nanotube resonator with the radio frequency signal applied to the current-carrying wire, the magnetic field gradient would be modulated a few kHz off the mechanical resonance as in Ref. [9]. By inverting the spins at a few kHz, the force, which is the product of the gradient and the magnetic moment of the spins, possesses a frequency component at the mechanical resonance. To further reduce the electrostatic drive, the wire would be symmetrically biased as in Ref. [9]. The radio frequency signal applied to the current-carrying wire may also broaden the Coulomb blockade peaks, thereby reducing the transconductance and the force sensitivity. This effect is difficult to estimate and therefore needs to be tested experimentally.

References

- [1] Choi, B.-R., Hansen, A. E., Kontos, T., Hoffmann, C., Oberholzer, S., Belzig, W., Schönenberger, C., Akazaki, T. & Takayanagi, H. Shot-noise and conductance measurements of transparent superconductor/two-dimensional electron gas junctions. *Phys. Rev. B* **72**, 024501 (2005).
- [2] Maizelis, Z. A., Roukes, M. L. & Dykman, M. I. Detecting and characterizing frequency fluctuations of vibrational modes. *Phys. Rev. B* **84**, 144301 (2011).
- [3] Lassagne, B., Tarakanov, Y., Kinaret, J., Garcia-Sanchez, D. & Bachtold, A. Coupling mechanics to charge transport in carbon nanotube mechanical resonators. *Science* **325**, 1107-1110 (2009).
- [4] Steele, G. A., Hüttel, A. K., Witkamp, B., Poot, M., Meerwaldt, H. B., Kouwenhoven, L. P. & van der Zant, H. S. J. Strong coupling between single-electron tunneling and nanomechanical motion. *Science* **325** 1103-1107 (2009).

- [5] Machlup, S. Noise in semiconductors: spectrum of a two-parameter random signal. *J. Appl. Phys.* **25**, 341 (1954).
- [6] Beenakker, C. W. J. *Phys. Rev. B* **44**, 1646 (1991).
- [7] Rugar, D., Budakian, R., Mamin, H. J. & Chui, B. W. Single spin detection by magnetic resonance force microscopy. *Nature* **430**, 329-332 (2004).
- [8] Degen, C. L., Poggio, M., Mamin, H. J., Rettner, C. T. & Rugar, D. Nanoscale magnetic resonance imaging. *Proc. Natl. Acad. Sci. USA.* **106**, 1313 (2009).
- [9] Nichol, J. M., Hemesath, E. R., Lauhon, L. J. & Budakian, R. Nanomechanical detection of nuclear magnetic resonance using a silicon nanowire oscillator. *Phys. Rev. B* **85**, 054414 (2012).
- [10] Nichol, J. M., Naibert, T. R., Hemesath, E. R., Lauhon, L. J. & Budakian, R. Nanoscale Fourier-transform MRI of spin noise. *arXiv:1302.2977*.
- [11] Poggio, M., Degen, C. L., Rettner, C. T., Mamin, H. J. & Rugar, D. Nuclear magnetic resonance force microscopy with a microwire rf source. *Appl. Phys. Lett.* **90**, 263111 (2007).